(Proceedings of the 5^{th} Technical Conference on Composite Materials, American Society of Composites, East Lansing, Michigan, June 11-14, 1990).

Fracture Mechanics Analysis of Composite Microcracking: Experimental Results in Fatigue

S. LIU AND J. A. NAIRN †

ABSTRACT

A recent variational mechanics analysis gives the energy release rate due to the formation of a new microcrack between two exisiting microcracks (John A. Nairn, *J. Comp. Mat.*, **23**, 1106 (1989)). This analysis has been useful in providing fracture mechanics interpretation of matrix microcracking in cross-ply laminates. This paper describes using the new energy relase rate analysis for a fracture mechanics based interpretation of microcrack formation during fatigue loading. Fatigue experiments were run of three layups of Avimid® K Polymer/IM6 laminates and on four layups of Fiberite 934/T300 laminates. A modifed Paris-law was used and the data from all layups of a single material system were found to fall on a single master Paris-law plot. We claim that the master Paris-law plot gives a complete characterization of a given material system's resistance to microcrack formation during fatigue laoding.

INTRODUCTION

Many observations have confirmed that the initiation of damage in multidirectional laminates is often by microcracks in the off-axis plies that run parallel to the fibers in those plies [1–8]. These microcracks have typically been studied in cross-ply laminates in which the cracks form in the 90° plies [1–8]. Microcracks form during static testing [1–8], during fatigue testing [3,9,10], and during thermal cycling [11]. Because microcracks cause a reduction in stiffness [3], a change in the thermal expansion coefficient [12,13], and provide sites for the initiation of delaminations, it is important to gain a quantitative understand of the formation and propagation of microcracks during both monotonic loading (static tests) and during cyclic loading (fatigue tests).

Some attempts at analysis of microcracking have been based on ply strength theories [2,14]. As pointed out by Flaggs and Kural [5], however, strength based theories are fundamentally inappropriate and most recent work has been based on energy release rate calculations [4,6,7,15–17]. Early energy release rate analyses were based on the shear-lag model [4,6,7,15] or on shear-lag type assumptions [16]. These types of analyses are probably too qualitative to be useful. A more recent energy release rate analysis [17] uses the improved stress analysis technique developed by Hashin [18,19]. The improved stress analysis is based on variational mechanics principles and has been shown to accurately predict stiffness reduction [18,19]. In Ref. [17] the variational approach was modifed to include thermal stresses and used to calculate the energy release rate due to the formation of microcracks. The new energy release rate analysis has been sucessuful in predicting the microcrack density as a function of applied load during static testing in a variety of composite material systems [17,20]. In this paper, we make further use of the new fracture analysis described in Ref. [17] to give a fracture mechanics interpretation of the propagation of microcracks during fatigue testing. The fracture mechanics interpretation is based on a modifed Paris-law approach.

† Graduate Student and Associate Professor, respectively, Materials Science and Engineering Department, University of Utah, Salt Lake City, Utah 84112

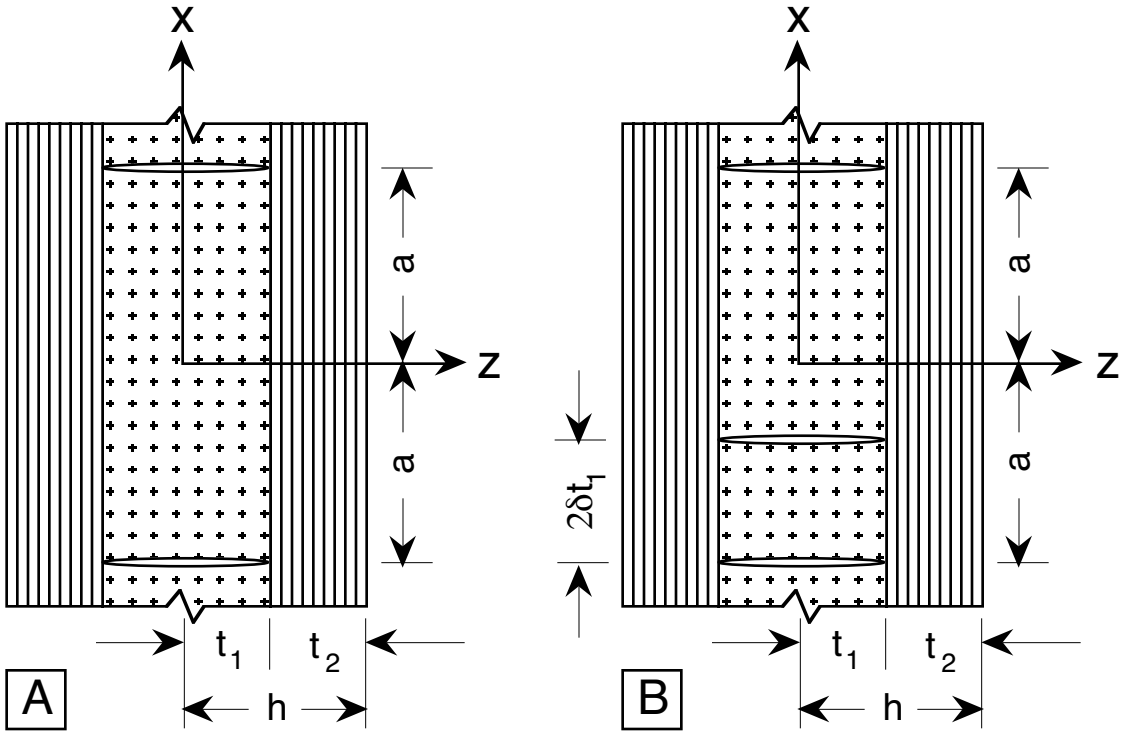

Figure 1: Edge view of a cross-ply laminate with microcracks. A: Two microcracks in the 90° plies. B: The formation of a new microcrack at a distance $2\delta t_1$ above the bottom microcrack.

MATERIALS AND METHODS

Fatigue experiments were run on two types of cross ply laminates of generic layup $[0_m/90_n]_s$. The first material system was supplied by DuPont and consisted of Avimid® K Polymer/IM6 graphite fiber laminates. These laminates were fabricated by DuPont using recently developed optimal processing techniques [21]. The second material system was provided by ICI/Fiberite and consisted of Fiberite 934 epoxy/T300 graphite fiber laminates. This material was supplied in prepreg form and was laminated by R-Cubed Composites in Salt Lake City, Utah, according to maufacturer's recommendations.

The fatigue tests were run on an MTS 25 kN servohydraulic testing frame using load control. The load span was set to cycle between a maximum stress, $\sigma_{\max}$, and small positive stress; in other words, the stress span, $\Delta\sigma_0$, was approximately equal to $\sigma_{\max}$. The cycling rate was usually 5 Hz. A few experiments were done using a lower rate of 1 Hz and the results were identical to the results at 5 Hz. During the fatigue test, the load cycling was periodically stopped and the microcrack density was measured by examining the sample edges under an optical microscrope and counting the cracks. The measurement was done on both edges of the flat specimens and the results were averaged. The sample dimensions were nominally 12 mm wide and 150 mm long; the thicknesses were determined by the stacking sequence.

FRACTURE ANALYSIS

Figure 1 shows the process of forming a new microcrack at some location between two existing microcracks. A recent thermoelastic variational mechanics analysis has been developed [17] which gives the total energy released due to the formation of the microcrack illustrated in Fig. 1. In this section, we summarize the analysis of Ref. [17].

Consider a laminate loaded by a tensile stress of σ_0 in the x direction. When that laminate is uncracked and at the stress free temperature, T_0, the only nonzero stresses will be the x axis tensile stresses in the 0° and 90° plies:

$$\sigma_{x0}^{(1)} = k_1\sigma_0 \qquad \text{and} \qquad \sigma_{x0}^{(2)} = k_2\sigma_0 \tag{1}$$

where k_1 and k_2 are effective stiffnesses and the supersripts (1) and (2) denote stresses in the 90° and 0° plies, respectively. The stiffnesses k_1 and k_2 can be found by laminated plate theory or, with sufficient accuracy, by a constant strain assumption whereby

$$k_1 = \frac{E_T}{E_c} \qquad \text{and} \qquad k_2 = \frac{E_A}{E_c} \tag{2}$$

In Eq. (2), E_A and E_T are the axial and transverse moduli of the ply material, and E_c is the x-direction modulus of the cross-ply laminate. Next change the temperature to T_s, the specimen temperature, and form the two cracks illustrated in Fig. 1A at $x = \pm a$. These changes will cause the stresses in the laminate to change. Following Hashin [18,19] we make one and only one assumption — that the x-axis tensile stresses in each ply depend only on the axial coordinate x and are independent of the thickness coordinate z. Under this assumption the stresses in the 90° and 0° plies will change to

$$\sigma_x^{(1)} = \sigma_{x0}^{(1)} - \psi_1(x) \qquad \text{and} \qquad \sigma_x^{(2)} = \sigma_{x0}^{(2)} - \psi_2(x) \tag{3}$$

where $\psi_1(x)$ and $\psi_2(x)$ are yet to be determined functions of x. By inserting the stresses in Eq. (3) into the stress equilibrium equations and making use of the obvious boundary conditions, it is possible to express all stresses in terms of $\psi(x) = \psi_1(x)$ [17–19]:

$$\begin{aligned}
&\sigma_x^{(1)} = \sigma_{x0}^{(1)} - \psi(x) && \sigma_{xz}^{(1)} = \psi'(x)z && \sigma_z^{(1)} = \frac{1}{2}\psi''(x)(ht_1 - z^2) \\
&\sigma_x^{(2)} = \sigma_{x0}^{(2)} - \frac{t_1}{t_2}\psi(x) && \sigma_{xz}^{(2)} = \frac{t_1}{t_2}\psi'(x)(h - z) && \sigma_z^{(2)} = \frac{t_1}{2t_2}\psi''(x)(h - z)^2
\end{aligned} \tag{4}$$

As can be verifed by substitution, the stress state in Eq. (4) satisfies equilibrium, traction boundary conditions, and interface stress continuity, and is therefore an admissible stress state. By the principal of minimum complementary energy, the function $\psi(x)$ that minimizes the complementary energy will give the best approximation to the cracked cross-ply laminate thermoelastic stress state. The complementary energy can be minimized using the calculus of variations. The final result, quoted from Ref. [17] is

$$\psi = \left(\sigma_{x0}^{(1)} - \frac{\Delta\alpha T}{C_1}\right)\phi + \frac{\Delta\alpha T}{C_1} \tag{5}$$

where $\Delta\alpha = \alpha_T - \alpha_A$ (the difference between the transverse and longitudinal thermal expansion coefficients), $T = T_s - T_0$, and ϕ is

$$\begin{aligned}
\phi = {} & \frac{2(\beta \sinh\alpha\rho \cos\beta\rho + \alpha \cosh\alpha\rho \sin\beta\rho)}{\beta \sinh 2\alpha\rho + \alpha \sin 2\beta\rho} \cosh\alpha\xi \cos\beta\xi \\
& + \frac{2(\beta \cosh\alpha\rho \sin\beta\rho - \alpha \sinh\alpha\rho \cos\beta\rho)}{\beta \sinh 2\alpha\rho + \alpha \sin 2\beta\rho} \sinh\alpha\xi \sin\beta\xi
\end{aligned} \tag{6}$$

In Eq. (6), $\rho = a/t_1$, $\xi = x/t_1$,

$$\alpha = \frac{1}{2}\sqrt{2\sqrt{q} - p} \qquad \text{and} \qquad \beta = \frac{1}{2}\sqrt{2\sqrt{q} + p} \tag{7}$$

Finally, $p = (C_2 - C_4)/C_3$, $q = C_1/C_3$, and the constants C_1 to C_4 are functions of the mechanical properties and thicknesses of the plies:

$$\begin{aligned}
C_1 &= \frac{hE_0}{t_2 E_A E_T} && C_2 = \frac{\nu_T}{E_T}\left(\lambda + \frac{2}{3}\right) - \frac{\lambda\nu_A}{3E_A} \\
C_3 &= \frac{\lambda + 1}{60E_T}\left(3\lambda^2 + 12\lambda + 8\right) && C_4 = \frac{1}{3}\left(\frac{1}{G_T} + \frac{\lambda}{G_A}\right)
\end{aligned} \tag{8}$$

The new terms in Eq. (8), G_A, G_T, ν_A, and ν_T, are the axial and transverse shear moduli and Poisson's ratio, respectively, and $\lambda = t_2/t_1$. Note that the above solution is specific for $4q/p^2 > 1$. This inequality

will hold for the composite specimens discussed in this paper. The solution for $4q/p^2 < 1$ is given in Ref. [17].

Before embarking on the fracture and fatigue analysis, we quote some additional results from Ref. [17]. Consider a sample with N microcracks characterized by crack spacings $\rho_1, \rho_2, \ldots, \rho_N$. The sample compliance is (*cf.* Eq. (38) in Ref. [17])

$$C = C_0 + \frac{E_T^2}{E_c^2}\frac{2C_3 t_1 L}{B^2 W}\frac{\sum_{i=1}^{N}\chi(\phi_i)}{\sum_{i=1}^{N}\rho_i} \tag{9}$$

where $B = 2h$ is the total thickness, W is the sample width (y-direction dimension), L is the sample length (x-direction dimension), and $C_0 = L/BE_cW$ is the compliance of the uncracked sample. The new function $\chi(\rho)$ for $4q/p^2 > 1$ is

$$\chi(\rho) = 2\alpha\beta\left(\alpha^2+\beta^2\right)\frac{\cosh 2\alpha\rho - \cos 2\beta\rho}{\beta\sinh 2\alpha\rho + \alpha\sin 2\beta\rho} \tag{10}$$

The result for $\chi(\rho)$ when $4q/p^2 < 1$ is given in Ref. [17]. The total strain energy in the N crack intervals is (*cf.* Eq. (43) in Ref. [17])

$$U = \left(\frac{\sigma_0^2}{2E_c} + \frac{t_1\Delta\alpha^2T^2}{BC_1}\right)BWL + (C-C_0)\frac{B^2W^2E_c^2}{2E_T^2}\left(\frac{E_T^2}{E_c^2}\sigma_0^2 - \frac{\Delta\alpha^2T^2}{C_1^2}\right) \tag{11}$$

Finally, the longitudinal thermal expansion coefficent of the cracked sample is

$$\alpha_L = \alpha_L^0 - \frac{C-C_0}{C_0}\frac{\Delta\alpha}{C_1E_T} \tag{12}$$

where α_L^0 is the longitudinal thermal expansion coefficient of the uncracked sample.

FRACTURE AND FATIGUE ANALYSIS

As suggested in Ref. [17] and other references [4,6,7,15,16], we assume that matrix microcracking is best modeled using an energy approach. By the energy approach to static testing, the next microcrack will form when the energy released on forming that crack reaches the critical energy release rate, G_{mc}, or the microcracking fracture toughness of the material system. To use the energy approach, we need an expression for the energy release rate — G_m. Consider the formation of a crack in the k^{th} crack interval as illustrated in Fig. 1B. The energy release rate associated with the formation of this crack can be found by differentiating Eq. (11) [22]:

$$G_m = -\left.\frac{\partial U}{\partial A}\right|_{\text{const. } u} = \frac{B^2W^2E_c^2}{2E_T^2}\left(\frac{E_T}{E_c}\sigma_0 - \frac{\Delta\alpha T}{C_1}\right)^2\frac{dC}{dA} \tag{13}$$

In deriving Eq. (13), we needed to evaluate $\left.\frac{\partial\sigma_0}{\partial A}\right|_{\text{const. } u}$. Using the relation for sample compliance times load of

$$CP = u(P) - u(0) = u(P) - \alpha_L LT \tag{14}$$

where $u(P)$ is sample displacement under load P, and differentiating results in

$$\left.\frac{\partial\sigma_0}{\partial A}\right|_{\text{const. } u} = \left(\frac{E_c\Delta\alpha T}{E_TC_1} - \sigma_0\right)\frac{1}{C}\frac{dC}{dA} \tag{15}$$

Eq. (15) corrects an error in Ref. [17] (*cf.* Eq. (44) in Ref. [17]) and accounts for the difference between Eq. (13) the corresponding equation in Ref. [17].

Evaluating $\frac{dC}{dA}$ by differentiating Eq. (9) results in the final energy release rate expression:

$$G_m = \left(\frac{E_T}{E_c}\sigma_0 - \frac{\Delta\alpha T}{C_1}\right)^2 C_3 t_1 Y(D) \tag{16}$$

where $Y(D)$ is a calibration function that depends on the crack density, $D = \frac{N}{L}$, or more formally on the complete distribution of crack spacings:

$$Y(D) = LW \frac{d}{dA} \frac{\sum_{i=1}^{N} \chi(\rho_i)}{\sum_{i=1}^{N} \rho_i} = \frac{d}{dD}\big(D\langle\chi(\rho)\rangle\big) \tag{17}$$

where $\langle\chi(\rho)\rangle$ is the average value of $\chi(\rho)$ over the N crack spacings.

To use Eq. (16), we must evaluate $Y(D)$. For the fracture process illustrated in Fig. 1 where a new crack forms at $\xi = 2\delta - \rho_k$ in the k^{th} crack interval characterized by ρ_k, we can evaluate $Y(D)$ by a discrete differentiation. Before the crack forms

$$\langle\chi(\rho)\rangle = \frac{1}{N} \sum_{i=1}^{N} \chi(\rho_i) \qquad \text{and} \qquad D = \frac{N}{L}.$$

After the crack forms

$$\langle\chi(\rho)\rangle = \frac{1}{N+1} \left[\left(\sum_{i=1}^{N} \chi(\rho_i) \right) - \chi(\rho_k) + \chi(\rho_k - \delta) + \chi(\delta) \right] \qquad \text{and} \qquad D = \frac{N+1}{L}.$$

The calibration function is therefore

$$Y(D) = \frac{\Delta\big(D\langle\chi(\rho)\rangle\big)}{\Delta D} = \chi(\rho_k - \delta) + \chi(\delta) - \chi(\rho_k) \tag{18}$$

During a typical experiment we will not know where the next microcrack will form. We do know, however, that cross-ply laminates tend to form regularly spaced microcracks. With regular spacings between the microcracks, the next microcrack will tend to form in a crack interval whose spacing is equal to the average crack spacing; in other words $\rho_k = 1/2t_1 D$. Furthermore, the tendency towards regular crack spacing indicates that the cracks tends to form in the middle of existing crack intervals and therefore $\delta = \rho/2$. With these two approximations

$$Y(D) = 2\chi(\rho/2) - \chi(\rho) = 2\chi\left(\frac{1}{4t_1 D}\right) - \chi\left(\frac{1}{2t_1 D}\right) \tag{19}$$

Eq. (16) along with the $Y(D)$ in Eq. (19) has been used to analyze data for the formation of microcracks during static testing [17,20]. The results are excellent. With a single microcracking fracture toughness, G_{mc}, for a given material system, it is possible to predict the microcrack density as a function of applied stress. More importantly, the same value of G_{mc} can be used to predict the very different results that are obtained from a variety of cross-ply laminates of generic structure $[0_m/90_n]_s$. More details on these experiments are given in Ref. [20].

In this paper, we describe some preliminary results of appplying Eq. (16) to the analysis of fatigue experiments. We propose to analyze fatigue data using a modified Paris-law [23] approach in which the rate of change in microcrack density is given by

$$\frac{dD}{dN} = A\Delta G_m^n \tag{20}$$

where A and n are two power-law fitting parameters. The conventional Paris-law approach relates the rate of change in crack length to the range in the applied stress intensity factor — ΔK. In the microcracking fracture experiment, the stress intensity factor approach is not possible and we have therefore substituted ΔG for ΔK.

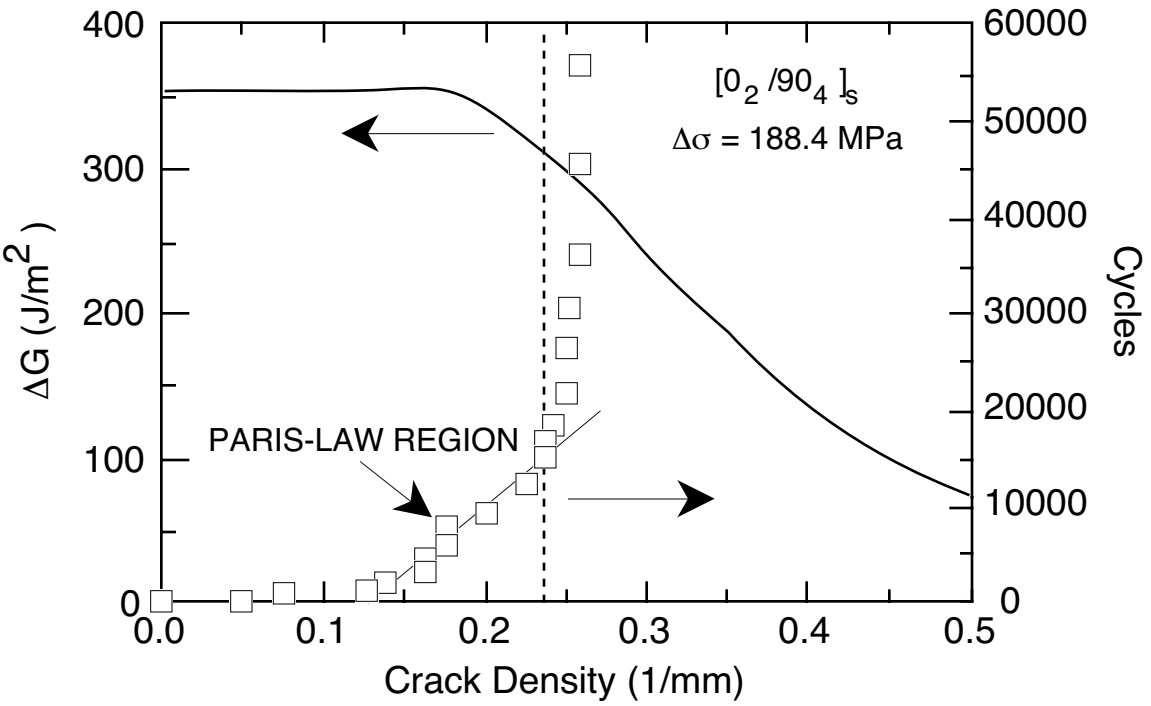

Figure 2: Microcracking fatigue data for a $[0_2/90_4]_s$ Fiberite 934/T300 composite. The solid line shows ΔG as a function of crack density. The symbols show the crack density as a function of cycle number. The straight line through the crack density data shows the Paris-law region of constant crack density growth rate.

RESULTS AND DISCUSSION

Our microcracking fatigue experiments were done under constant amplitude load conditions. With a given $\Delta\sigma_0$ at a given crack density, it is a simple matter to calculate ΔG using Eq. (16). If Eq. (20) is valid, plotting $\frac{dD}{dN}$ as a function of ΔG on a log-log plot should yield a linear relation. The problem with most fatigue crack propagation experiments is that during the experiment, both the dependent variable (crack length) and the independent variable (ΔK) change. A fortunate feature of microcracking fatigue experiments, however, is that the dependent variable (ΔG) remains constant up to reasonably high crack densities. Figure 2 plots ΔG as a function of crack density for a typical fatigue experiment on a $[0_2/90_4]_2$ Fiberite 934/T300 composite. ΔG is constant up to a crack density of about 0.20–0.25 mm^{-1} and then drops rapidly to a low value.

Because ΔG is constant over a fairly wide range, we can do relatively simple fatigue microcrack propagation experiments. We measure the crack density as a function of cycle number for various values of $\Delta\sigma_0$. Up to values of the crack density of about 0.20–0.25 mm^{-1}, ΔG is constant and we expect by Eq. (20) that the crack density will increase linearly with cycle number. Typical experimental results are given in Fig. 2. For this sample there is a region of linear density increase between crack densities of 0.13 mm^{-1} and 0.23 mm^{-1}. In agreement with Paris-law behavior, the crack density stops increasing after it reaches 0.25 mm^{-1} which corresponds to the density at which ΔG begins its rapid decline.

Contrary to Paris-law behavior, however, there is a rapid increase in crack density up to 0.13 mm^{-1} that occurs before the linear Paris-law growth region. We suggest that these cracks are a result of inherent flaws in the laminate. Similar observations were made during static experiments in which some cracks typically form at loads well below the loads predicted by the fracture toughness of the material system [20]. In those experiments, the early cracks were observed using microscopy and were normally found to be located near obvious flaws. With the above comments, we divide the crack density vs. cycle number data into three regions:

1. **Flaw Dominated Region:** The first few microcracks form during the first few cycles and form at flaws. The formation of these microcracks are controlled by laminate quality. The energy release

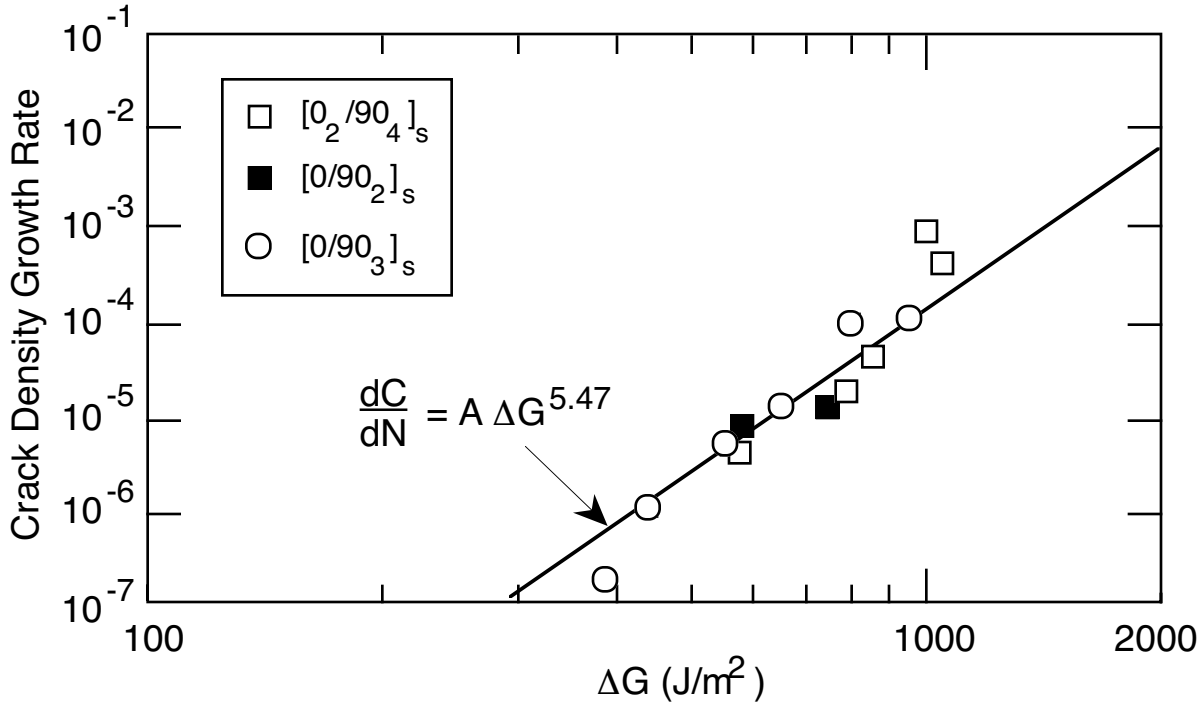

Figure 3: The crack density growth rate (in cracks per mm per cycle) as a function of applied ΔG for Avimid® K Polymer/IM6 laminates. As indicated on the figure, the results are from three different cross-ply layups.

rate in Eq. (16) does not account for macroscopic flaws and therefore can not be used to predict the behavior in this region.

2. **Constant Growth Region:** After the inherent flaws are used up, the crack density increases according to the Paris law in Eq. (20). Up to a crack density of about 0.25 mm^{-1} (depending on laminate properties and the thicknesses of the 0° and 90° plies), ΔG remains relatively constant and therefore the crack density increases at a constant rate. The crack formation in this region is controlled by the inherent toughness of the material system.

3. **Slow Growth Region:** At high crack densities, ΔG decreases. According to the Paris-law in Eq. (20), this decrease will cause a dramatic reduction in the crack formation rate.

To map out the resistance of a composite material system to fatigue induced microcracking involves measuring the crack density growth rate as a function of applied ΔG. These experiments are most conveniently done in the constant growth region. In brief, we subject various cross-ply laminates to various levels of $\Delta\sigma_0$ and measure the crack density as a function of cycle number. Before starting the experiment, we can use Eq. (16) to calculate the crack density at which ΔG begins to decrease. We run our experiments up to this crack density and look for the constant crack growth region. We always observe a constant crack growth region and the slope in this region gives the crack density growth rate. Finally, we plot this growth rate vs. ΔG to obtain a fatigue resistance plot.

The first microcrack fatigue resistance experiments were done on Avimid® K Polymer/IM6 laminates and the results are in Fig. 3. We note four things about the results:

1. Over a fairly wide range in ΔG the log-log plot is linear indicating that Eq. (20) holds. The power-law exponent in the linear region is $n = 5.47$.

2. At very high ΔG the microcracks propagate very fast. This upper limit occurs at a $\Delta G \approx 1000$ J/m^2 which is very near to the static microcracking fracture toughness of these laminates which has been measured to be 920 J/m^2 [20].

3. The lowest ΔG data point falls below the Paris-law line. This may be an indication of a threshold

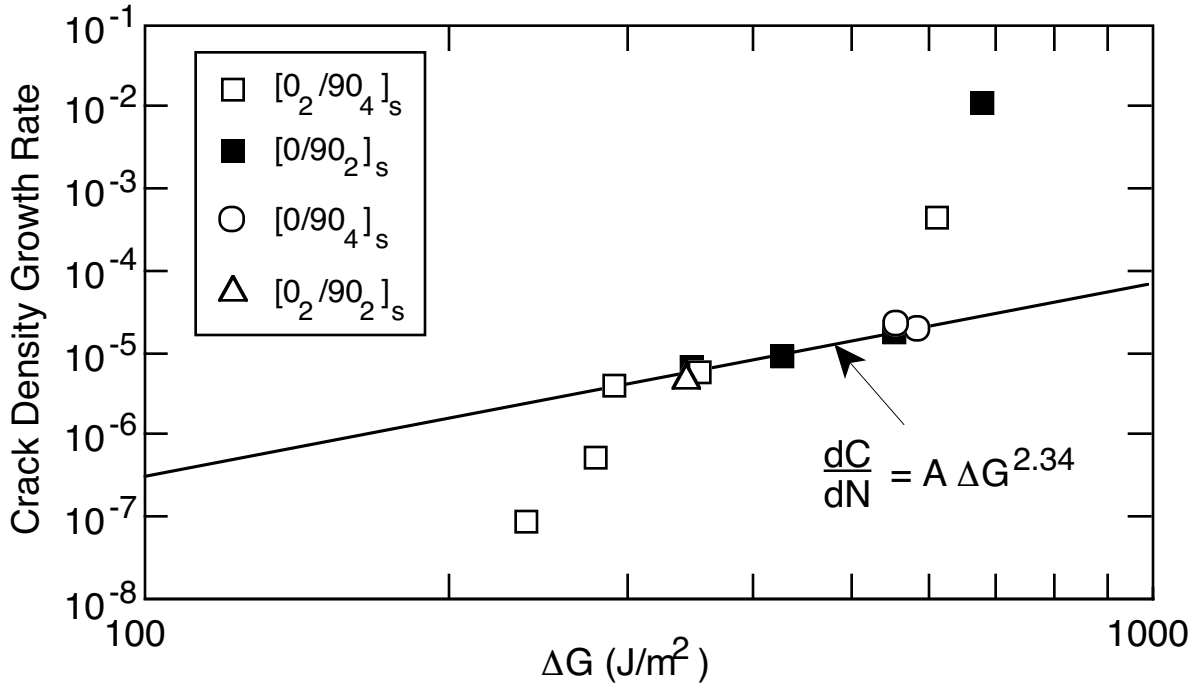

Figure 4: The crack density growth rate (in cracks per mm per cycle) as a function of applied ΔG for Fiberite 934/T300 laminates. As indicated on the figure, the results are from four different cross-ply layups.

limit to fatigue induced microcracking occurring at about 400 J/m^2.

4. Perhaps most important, as indicated in Fig. 3, we note that the data came from three different layups — $[0_2/90_4]_s$, $[0/90_2]_s$,and $[0/90_3]_s$ laminates. Although the raw data differ from laminate to laminate, we have been able to reduce all experimental results to a single master Paris-law plot by normalizing to the applied energy release rate as calculated by Eq. (16). As has been observed during conventional fatigue crack propagation experiments [24], the master Paris-law plot has a linear region that corresponds to the power law in Eq. (20), and has indications of a thresold limit at low ΔG and of fast fracture at high ΔG. This result supports an energy based fracture mechanics view of composite microcracking. In principal, this master Paris-law plot could be used to predict the propagation of microcracks in a variety of Avimid® K Polymer/IM6 laminates.

A second set of experiments was run on Fiberite 934/T300 laminates; the results are given in Fig. 4. We again note a linear Paris-law region with a power-law exponent of $n = 2.34$. The linear region is much shorter for Fiberite 934/T300 laminates than it was for the Avimid® K Polymer/IM6 laminates. At high ΔG (about 650 J/m^2) we see rapid propagation of microcracking. This high ΔG is close the static microcracking fracture toughness of these laminates which has been measured to be 690 J/m^2 [20]. The two lowest ΔG points suggest a threshold limit for microcracking of about 250 J/m^2. Finally, as indicated in Fig. 4, the data came from four different layups — $[0_2/90_4]_s$, $[0_2/90_2]_s$, $[0/90_2]_s$, and $[0/90_4]_s$ laminates. The fact that all this data falls on a single Paris-law plot supports our hypothesis that Eq. (16) gives a useful fracture mechancics interpretation of composite microcracking.

ACKNOWLEDGEMENTS

This work was supported in part by a contract from NASA Langley Research Center (NAS1-18833) monitored by Dr. John Crews, and in part by a gift from the Fibers Department of E. I. duPont deNemours & Company monitored by Dr. Alan R. Wedgewood.

REFERENCES

1. H. T. Hahn and S. W. Tsai, *J. Comp. Mat.*, **8**, 288 (1974).
2. K. W. Garret and J. E. Bailey, *J. Comp. Mat.*, **12**, 157 (1977).
3. A. L. Highsmith and K. L. Reifsnider, *ASTM STP*, **775**, 103 (1982).
4. A. Parvizi, K. W. Garrett, and J. E. Bailey, *J. Mat. Sci.*, **12**, 195 (1978).
5. D. L. Flaggs and M. H. Kural, *J. Comp. Mat.*, **16**, 103 (1982).
6. M. G. Bader, J. E. Bailey, P. T. Curtis, and A. Parvizi , *Proc. 3^{rd} Int'l Conf. on Mech. Behavior of Materials*, **3**, 227 (1979).
7. J. E. Bailey, P. T. Curtis, and A. Parvizi, *Proc. Roy. Soc. London*, **A366**, 599 (1979).
8. S. E. Groves, C. E. Harris, A. L. Highsmith, and R. G. Norwell, *Exp. Mech.*, 73 (March, 1987).
9. L. Boniface, P. A. Smith, S. L. Ogin, and M. G. Bader, *Proc. 6^{th} Int'l Conf. on Composite Materials*, **3**, 156 (1987).
10. L. Boniface and S. L. Ogin, *J. Comp. Mat.*, **23**, 735 (1989).
11. C. T. Herakovich and M. W. Hyer, *Eng. Fract. Mech.*, **25**, 779 (1986).
12. D. S. Adams and C. T. Herakovich, *J. Thermal Stresses*, **7**, 91 (1984).
13. D. E. Bowles, *J. Comp. Mat.*, **17**, 173 (1984).
14. P. W. Manders, T. W. Chou, F. R. Jones, and J. W. Rock, *J. Mat. Sci.*, **18**, 2876 (1983).
15. D. L. Flaggs, *J. Comp. Mat*, **19**, 29 (1985).
16. Y. M. Han, H. T. Hahn, and R. B. Croman, *Proc. of the Amer. Soc. Composites, Second Technical Conf.*, Newark, DE (September 23–25, 1987).
17. J. A. Nairn, *J. Comp.Mat.*, **23**, 1106 (1989).
18. Z. Hashin, *Mechanics of Materials*, **4**, 121 (1985).
19. Z. Hashin, *Eng. Fract. Mech.*, **25**, 771 (1986).
20. S. Liu and J. A. Nairn, *J. Comp. Mat.*, submitted.
21. A. R. Wedgewood and D. C. Grant, 34^{th} *Int'l SAMPE Technical Conf.*, **19**, 454 (1989).
22. J. G. Williams, *Fracture Mechanics of Polymers* (John Wiley & Sons, New York, 1984).
23. P. Paris and F. Erdogan, *J. Bas. Eng. Trans. ASME, Ser. D*, **85**, 528 (1963).
24. R. W. Hertzberg and J. A. Manson, *Fatigue of Engineering Plastics* (Academic Press, New York, 1980).